Alumina scale composition and growth rate in distribution pipes

Ingrid Bokn Haugland[1,2], Ole Kjos[1], Arne Røyset[1], Per Erik Vullum[1], Thor Anders Aarhaug[1], Maths Halstensen[2]

1. SINTEF Industry, P.O Box 4760 Torgarden, N-7465 Trondheim, Norway
2. Faculty of Technology, Natural Sciences and Maritime Sciences, University of South-East Norway, P.O Box 203 N-3901, Porsgrunn, Norway

Keywords: Alumina, scaling, pneumatic conveying, aluminium smelter, multivariate data analysis

Abstract

Scaling in distribution pipes for secondary alumina is a major issue in aluminium smelters. The scale is formed inside the distribution pipes, and gradually reduces the cross section that is available for alumina transport. The scale cannot be removed without dismantling the transport pipes and using chemical and/or mechanical treatments. This leads to interruptions in normal operation, requires additional labour, and a stock of additional pipe sections. To get a better understanding of the scale formation mechanisms, the rate of scale growth was monitored by acoustic measurements in a transport pipe section at an aluminium producing plant over a period of several months. Correlation between growth rate, and recorded parameters from the associated pots, fume treatment system and meteorological data were studied. In addition, samples from the actual scale were examined by SEM, TEM and AFM to investigate the microstructure and chemical composition.

Introduction

Hard grey scale (HGS) is a material that deposits in secondary alumina distribution systems. It is a major maintenance issue in many plants, leading to increased operational costs and process interruptions. In general, HGS is observed in the dry-scrubbers and downstream of them: in the delivery pipes transporting secondary alumina to the production cells. HGS is not observed in the primary alumina distribution pipes. It can therefore be assumed that some of the adsorbed components and/or the handling occurring in the dry-scrubber contributes to the scale formation.

There are very few publications available in the literature addressing scale formation in secondary alumina distribution pipes. The most extensive investigation was presented in [1]. They showed that a hard grey scale could be synthetized using bath fines, alumina and water which were mixed in a ball mill. All of these components had to be present in the right amount, in addition to the energy from the ball mill, for scale to form in the study. Investigations of the necessary conditions for scale formation revealed an increase in the temperature of about 15-20 °C when scale formed.

Possible mechanisms for scale formation

For scale to form, secondary alumina particles must adhere to the pipes and grow into thick layers. This could be caused by either pure particle to particle interactions, a binder phase between particles or a recrystallisation of particles that enables them to grow into each other by a mechanism like sintering.

Temperature could be an important parameter for such reactions. Recrystallisation is slowed down or stopped at lower temperatures. A binder phase must be ductile or liquid, usually meaning it must be close to its melting point. This can explain why scaling tends to occur at high-turbulence areas, as the energy from the impacts can give increased local temperature on involved particles. Some proposed contributions to scale formation is discussed in more details below.

Fluoride salts

Fluoride containing fines originating from bath fumes are present in high amounts in the secondary alumina. Fluorides from HF and bath fumes are captured by the alumina as it passes through the gas scrubber. A study showed that $Na_5Al_3F_{14}$ (chiolite) and Na_3AlF_6 (cryolite) could be synthesised from AlF_3 and NaF at ambient temperature using a high energy ball mill [2]. Thus, it was proved that fluoride salts can undergo solid state

chemical reactions under these conditions. A similar reaction between the fluoride species available in the secondary alumina might lead to a recrystallisation of the fluorides which could result in crystal growth and a rearrangement of the crystalline structure such that it locks the neighbouring particles in place.

Na_2O and NaOH

Alumina from refineries have a high content of Na_2O, typically around 0.5%. Although co-precipitated with the gibbsite during the Bayer process, it was showed in [3] that Na_2O emerges to the surface of the alumina grains during calcination. Na_2O is thermodynamically unstable when exposed to moisture and air and will react to form NaOH or Na_2CO_3 in the presence of H_2O or CO_2. NaOH, with a melting point of 318 °C, have the potential to melt in a high energy impact.

Alumina recrystallisation

Reports [1,4,5] show that high amounts of alpha phase alumina can be found in the scale. A possible reason for this could be recrystallisation of γ-Al_2O_3, which again could lead to a sintering / agglomeration taking place during the rearrangement of the crystal structure.

Geopolymers

Geopolymers, or hydraulic cements, is another form of inorganic compounds that bind together directly. Many of these suggested geopolymers contain aluminium oxides. They typically consist of structures made of Si-Al-O, or Al-P-O. The absence of Si (and P) which is key ingredients in geopolymer structures rules out this option as a scale formation mechanism. The initial formation of precursors i.e. the formation of Si-Al-O structure from SiO_2 and Al_2O_3, would also require high temperature (typically 1000 °C or higher), although the actual solidification of a geopolymer could occur at ambient temperatures [6].

Sulphate

Sulphate can form solid phases with many common cations such as Ca^{2+}, Na^{+}, and sulphur is present in the off-gas entering the dry scrubber mainly as SO_2. SO_2 is known to adsorb on alumina. According to [7], SO_2 can react with sodium doped alumina to form sodium sulphate, also known as gypsum. Gypsum, or any gypsum like substances could, given the right moisture conditions, solidify and act as a binder phase.

Zhang et al. studied the reactions of sulphur dioxide on alumina, and showed that given the right conditions SO_2, would adsorb non-reversibly to form SO_3^{2-}, and could further react to from SO_4^{2-} [8]. Kogarkoite ($Na_3(SO_4)F$) has been identified as fumes in the off gas from electrolysis cells [9].

Humidity

Alumina will have a moisture uptake and equilibrium affected by calcination, air temperature and relative humidity. Changes in moisture in the alumina can result in changed flowability and other physical properties and is hence a parameter that could affect the scale formation. In addition, the moisture level has at higher temperatures (6-800 °C) shown to affect agglomeration and neck formation of alumina agglomerates [10]. It was also found in [1] that without some water additions in the ball mill scale did not form.

Particle collisions

Alumina is transported using pressurized air in distribution pipes (pneumatic conveying). HGS growth is reported to be larger in high turbulence areas, where collisions between particles and pipe walls as well as high energy particle-particle collisions can be expected. These collisions can lead to breakdown of particles, with exposure of a highly reactive fracture surface which will reorganize, often reacting with moisture in air in an exothermic reaction which also can give rise to significant local heat [1]. Additionally, the kinetic energy itself from the collision can theoretically give a temperature increase of $dT = 0{,}5v^2/Cp$, where v is velocity in m/s and Cp is the heat capacity in J/(g*K). Given a particle impact at 15m/s the theoretic heat increase is 128 °C if all the kinetic energy is converted to heat, this additional heat could be what enables the scale forming reactions by melting of a binder product that is otherwise solid.

Methodology

This paper discusses scale formation based on measurement of scale progression during a five-month long monitoring campaign, combined with analysis of process and environmental variables in addition to chemical analysis of the scale.

Measurements of scale growth

A methodology for measuring scale growth in a pipe was established in previous studies [11,12]. An acoustic method was used to monitor the scale growth in a test area along a pneumatic conveying system distributing secondary alumina in a Norwegian smelter. Reference measurements to calibrate models from the acoustic signals were collected with a laser/camera setup on a weekly basis. The main results from the monitoring campaign and development of calibration models of the scale growth is discussed in detail in [13].

Multivariate data analysis

Latent variable methods

Multivariate data is typically presented in an *m***n* matrix **X** and is often colinear as the columns in **X** are linearly dependent of each other to some extent. In such cases, some of the same underlaying factors are described by several of the different variables in the dataset. Thus, a smaller set of variables describing the same information can be constructed by linear combinations of the variables in **X**. The new variables are referred to as latent variables (LVs) as they contain the main underlaying or hidden structures in the original data. Latent variables can be constructed by an iterating process of successive orthogonal projections as described in eq. 1-3 (NIPLAS algorithm).

Each LV is represented by a score vector **t** and a loading vector **p**. The score vector is calculated by defining a weight vector $\mathbf{w}_a$ and projecting the rows of the matrix **X** onto $\mathbf{w}_a$ as shown in Eq. 1.

$$\mathbf{t}_a = \mathbf{X}_a \mathbf{w}_a \tag{1}$$

Subsequently, the loading vector $\mathbf{p}_a$ is found by projecting the variables in **X** onto the $\mathbf{t}_a$ vector as described in Eq. 2.

$$\mathbf{p}_a = \frac{\mathbf{t}_a^{\mathrm{T}} \mathbf{X}_a}{\|\mathbf{t}_a^{\mathrm{T}} \mathbf{X}_a\|} \tag{2}$$

Finally, the variation described by LV_a is removed from **X** as defined in Eq. 3. In Eq. 1-3, a = 1, 2, …, A and $\mathbf{X}_1$ = **X**.

$$\mathbf{X}_a = \mathbf{X}_{a-1} - \mathbf{t}_{a-1} \mathbf{p}_{a-1}^{\mathrm{T}} \tag{3}$$

A maximum of A = rank (**X**) LVs can be calculated by this procedure. However, normally the main variations in **X** can be described by only a few latent variables. Thus, the important information in **X** is summarized in a few components, significantly reducing the dimension of the dataset and simplifying the interpretation of the data. By calculating LVs, the **X** matrix is decomposed into an information part (LVs) and a noise part (the residual matrix **E**) as shown in Eq. 4.

$$\mathbf{X} = \mathbf{t}_1 \mathbf{p}_1^{\mathrm{T}} + \mathbf{t}_2 \mathbf{p}_2^{\mathrm{T}} + \cdots + \mathbf{t}_a \mathbf{p}_a^{\mathrm{T}} + \mathbf{E} \tag{4}$$

Several different types of latent variable methods exist, Eq. 1-4 are common for all. The methods differ in the choice of weights $\mathbf{w}_a$ and thus the properties of the LVs [14].

Before conducting the latent variable matrix decomposition, the data in **X** is normally pre-processed by various techniques to adapt and prepare it for the data analysis. A common pre-processing technique called autoscaling involves mean centring and scaling the columns in **X** to unit length [15].

Partial least squares regression

Partial least squares regression (PLS-R) is a latent variable method used to find linear correlation models between a set of predictor variables (**X**) and response variables (a single variable **y** in PLS1, the version of PLS-R discussed in this paper). PLS-R is the most commonly used regression method for multivariate data as it can

handle datasets containing noisy and colinear variables. The method solves the calibration equation in Eq. 5 by finding a set of regression coefficients **β** that relates **X** to **y** and minimizes the residual vector **ϵ**.

$$\mathbf{y} = \mathbf{X}\boldsymbol{\beta} + \boldsymbol{\epsilon} \tag{5}$$

In PLS-R, the weight variable used in Eq. 1 is defined as shown in Eq. 6.

$$\mathbf{w}_a = \frac{\mathbf{y}_a^{\mathrm{T}}\mathbf{X}_a}{\|\mathbf{y}_a^{\mathrm{T}}\mathbf{X}_a\|} \tag{6}$$

The choice of $\mathbf{w}_a$ results in LVs being calculated according to a criterium of maximum covariance between **X** and **y**. Thus, in PLS-R the information that is most relevant to describe the relation between **X** and **y** is extracted. More detailed descriptions of PLS-R can be found in [15,16].

Variable selection by variable importance in projection

When calibrating PLS-R models, it is often found that many of the variables in **X** are not contributing significantly in modelling **y**. Variable selection methods can be used to evaluate which variables seems important and which variables seems insignificant. Removing unimportant variables from **X** can often lead to improved model performance due to noise reduction and will also simplify the model interpretation. Numerous different variable selection techniques exist, and the best choice of method will depend of the properties of the investigated dataset. Variable importance in projection (VIP) is a variable selection method which gives an evaluation of the contribution of each variable in a dataset to describe **X** and **y**. The VIP value for a variable *j* in **X** (*j* = 1, 2, …, *n*) can be calculated as described in Eq. 7.

$$\mathrm{VIP_j} = \sqrt{\sum_{a=1}^{A} \frac{\mathbf{w}_{ja}^2 * \boldsymbol{\beta}_a^2 \mathbf{t}_a^{\mathrm{T}} \mathbf{t}_a}{\boldsymbol{\beta}^2 \mathbf{T}^{\mathrm{T}} \mathbf{T}}} \tag{7}$$

In Eq. 7, **T** refers to a score matrix containing the score vectors for all the LVs included in the PLS-R model. As a rule of thumb, VIP-values lower than one are regarded as insignificant [17].

Experimental

Multivariate data analysis of a dataset containing multiple variables was conducted to reveal any correlation between the variables and scale formation. Several parameters were evaluated, including meteorological parameters such as dewpoint, air temperature and amount of rainfall (weather forecast from Yr, delivered by the Norwegian Meteorological Institute and NRK) as well as process data from the aluminium production pots and the gas treatment centre (GTC) connected to the pipeline where the measurement campaign was performed. The aluminium production data consisted of average values for all pots in the potline in the relevant area of the plant. The data was arranged in a matrix in which the rows each represent a day in the test campaign and the columns corresponds to the process and environmental variables. The data was auto scaled prior to the analysis.

PLS-R modelling, with the investigated parameters as predictors and a pre-processed scale growth curve obtained from the measurement campaign as the response, was carried out. A combination of the VIP variable selection method applied to the resulting PLS-R model and a correlation analysis of the variables in **X** was used to determine the main influential parameters for scale growth. A T-test was applied to check if the calculated correlation coefficients were significantly different from zero. The data analysis was conducted using Sirius [18].

Analysis of scale samples

The analysis of scale was done using a combination of SEM and TEM to get high resolution combined with chemical analysis. AFM analysis was used to evaluate the physical properties. The instruments used was a FEI Helios G4 dual-beam focused ion beam – scanning electron microscope (FIB-SEM) and a double Cs corrected coldFEG JEOL ARM 200F, operated at 200 kV and equipped with a large solid angle Centurio (0.98 sr solid angle) detector for X-ray Energy Dispersive Spectroscopy (EDS) and a Quantum ER GIF for electron energy loss spectroscopy (EELS). The FIB-SEM was used both for standard SEM characterization and to make samples for TEM. Samples for SEM were cut with a diamond impregnated cutting blade and further polished with SiC paper and diamond coated plastic lapping films (finishing with a diamond grain size of 0.5 µm) prior to FIB-SEM characterization. The TEM samples were made by standard lift-out and transfer of the TEM lamella to a dedicated

Omniprobe TEM grid. Coarse thinning was performed at 30 kV ion beam acceleration voltage. Final thinning was done at 5 and 2 kV to minimize the surface damage on either side of the TEM lamella.

The AFM instrument used was a Veeco diMultimode V in PeakForce QNM (Quantiative Nanomechanical Mapping) operation mode. In QNM mode, topography is acquired together with additional information on modulus, adhesion deformation and dissipation. The QNM information is a result of the deformation vs force analysis provided by the NanoScope8.15 software. The AFM tip was a Bruker Scanasyst-air silicon tip with a nominal tip radius 2nm and spring constant 0.4N/m.

Results

The methodology proved successful in monitoring scale progression and provided detailed information of scale growth during the test campaign. A curve showing the scale growth in this period, which was generally steadily increasing, is plotted in Figure 1. There are some fluctuations and periods of time where the growth seems to stop or reverse. The latter could be caused by abrasion by alumina on the scale in timeframes where the growth is low or by chip-off of scale pieces resulting from mechanical influence. The curve was detrended and smoothed (Figure 1) to emphasize the main changes in scaling rate throughout the test campaign. The pre-processed curve was used as the response variable in the data analysis in order to focus on the sub trends with increasing and decreasing scaling rate. If the original scale growth curve had been used in the analysis, the results would be dominated by variables with a general increasing trend that may not have any relation to scale growth.

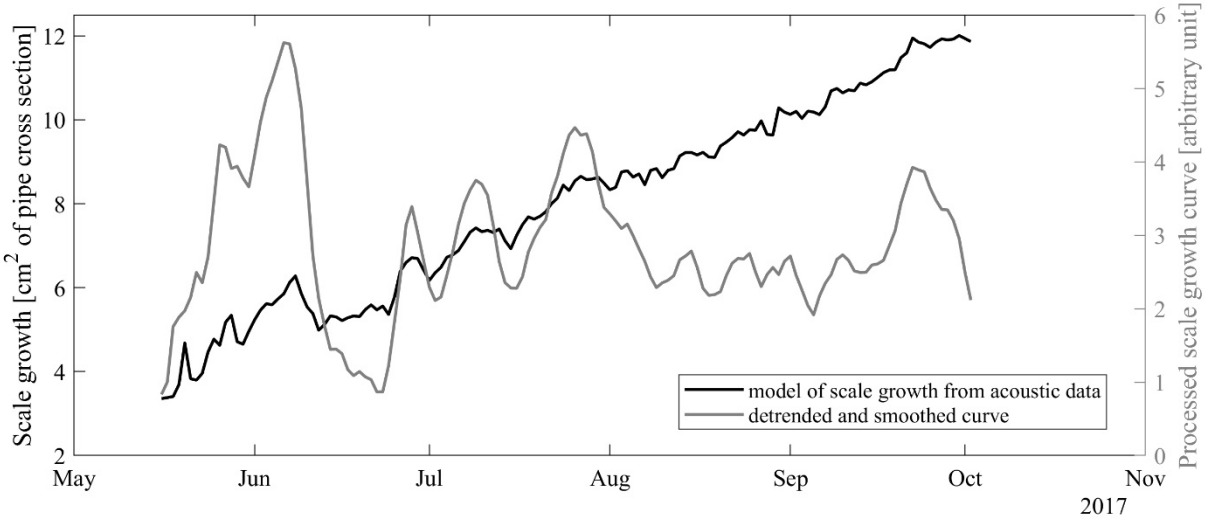

Figure 1: Scale growth as a function of time (black curve) and a pre-processed version of the curve highlighting sub trends of increasing and decreasing scale growth rate (grey curve).

Multivariate data analysis to detect variables correlated to scale formation

Investigating correlations between scale growth and other parameters have been a challenging task for several reasons. Process data from aluminium production is known to be temporally correlated [19], and complex co-dependencies probably exist between the variables, complicating the analysis. Furthermore, the dataset investigated in this study was relatively small, representing a few months of production only. The calibrated model's ability to represent the scale growth is restricted by the availability of reference measurements, and relatively few such measurements could be carried out in the test campaign [13]. Also, the variables were scaled to unit variance, which can lead to unimportant variables mainly containing noise getting an artificially high influence on the calibrated models [15]. Finally, key variables influencing scaling may not have been present in the dataset and if so, could not be detected by the analysis.

Nevertheless, several groups of variables which seems to be correlated to scale formation, presented in Table 1, were found in the data analysis. These variables were considered carefully to investigate whether there could be any connection to scaling as correlation does not necessarily mean there is a cause-effect relationship between variables. Many of the variables in Table 1 are mutually correlated and it is likely that they are all related to some common underlaying factors which are influencing scaling and making the variables stand out in the

analysis. Most of the variables in Table 1 have a connection to cell emissions, cell temperature and/or gas temperature, these could be the main parameters that are affecting the scale formation.

Table 1: Overview of variables found to be correlated with scale formation

Group	Variable	VIP	r
1	Anode effects in cells	1.27	0.327
2	Measured resistance	1.22	0.332
	Cell to cell voltage	1.21	0.327
	Series voltage	1.19	0.225
3	Bath height	1.17	0.325
	Liquid height	1.15	0.324
4	Na_2CO_3 addition to bath	1.18	0.318
5	Max outdoors air temperature	1.07	0.271
	Gas temperature in and out of GTC	1.07	0.260
6	Iron in produced metal	1.05	0.242

Although the correlation coefficients in Table 1 are relatively low, they are all statistically significant ($\alpha = 0.05$) due to the high number of samples in the dataset. The VIP values are all above 1, thus the variables are considered important according to the VIP test criterium.

Normally consisting mostly of CO_2, the off-gas composition shifts towards higher contents of CO, CF_4, and some C_2F_6 during anode effects. Furthermore, anode effects involve rapid rise in cell voltages and resistance, temperature rise in the cells, higher emission rates and higher gas temperatures. Accordingly, the variables in group 2 are correlated to group 1. Additionally, the group 2 variables are connected to general temperature changes in the pots, which is one of the main factors affecting the total fluoride emission from the cells [21]. The variable describing cell temperature itself did not stand out in the data analysis, this is believed to be a consequence of the usage of average values for all pots in the analysis. As the change in vapor pressure is not linearly correlated to the temperature changes, smaller changes in process temperature in individual cells, which are not detectable in the calculated mean value of all cell temperatures, could have a significant impact on the total fluoride emission.

The effect of the variables in group 3 could possibly be explained by a relation to changes in anode to cathode distance and thereby to group 2 variables. However, as cell operation strives to keep the inter-polar distance at a constant level, such variations may be too minor to have a significant effect on the cell conditions. Another possibility is that higher bath and liquid heights could lead to higher cell emissions.

Several long episodes of anode effects resulting from the start-up of two new production pots were registered during the test campaign, in mid-May and early June. Interestingly, it can be seen from Figure 1 that the scaling rate increased drastically during these periods. Major changes in the variable in group 4 was found for the same periods, probably caused by significant additions of Na_2CO_3 to the start-up cells. Thus, the variable in group 4 is related to anode effects and consequently it is indirectly correlated to the main factors mentioned above.

The influence of the group 6 variables is harder to determine. It is possible that the correlation is indirect and that the underlaying factor affecting scaling is the fines content in secondary alumina, as iron, vanadium and manganese as well as other contaminants has been found to accumulate in the finer fractions of alumina [22].

Surprisingly, no correlation was found between scale growth and humidity. However, due to the challenges of the data analysis as explained in the start of this paragraph, a connection between humidity and scaling cannot be ruled out based on the results in this study.

To summarize, the multivariate analysis indicates that cell emissions, gas temperature, production temperature in individual cells and possibly the content of fines in the alumina is affecting scale growth, although no strict conclusions can be drawn at this stage. To validate the results, a new, similar study needs to be conducted and data analysis needs to be performed to check whether the main influential variables found in the new study agree with Table 1.

SEM and TEM analysis of scale samples

When the test pipe from which measurements had been obtained was due to be replaced, it was collected as a sample and conserved to analyse the scale while it was attached to the pipe wall. Additional samples of scale from the pipes were also obtained and conserved in sealed plastic bags. Examinations using SEM, TEM and AFM were carried out.

From the SEM analysis it was possible to observe the interface between the steel pipe and the actual scale. This can be seen in Figure 2. The plan was originally to take TEM samples of the pipe-scale interface to look for clues on how the scale binds to the steel pipe, but interestingly, on all 3 samples that were analysed at the interface, there seemed to be a corrosion layer of the pipe between the scale and the metal. This made it impossible to extract a sample from this area. It could not be determined if the corrosion was a result of chemical reactions with the scale, or if the scale preferentially grows on a corroded surface.

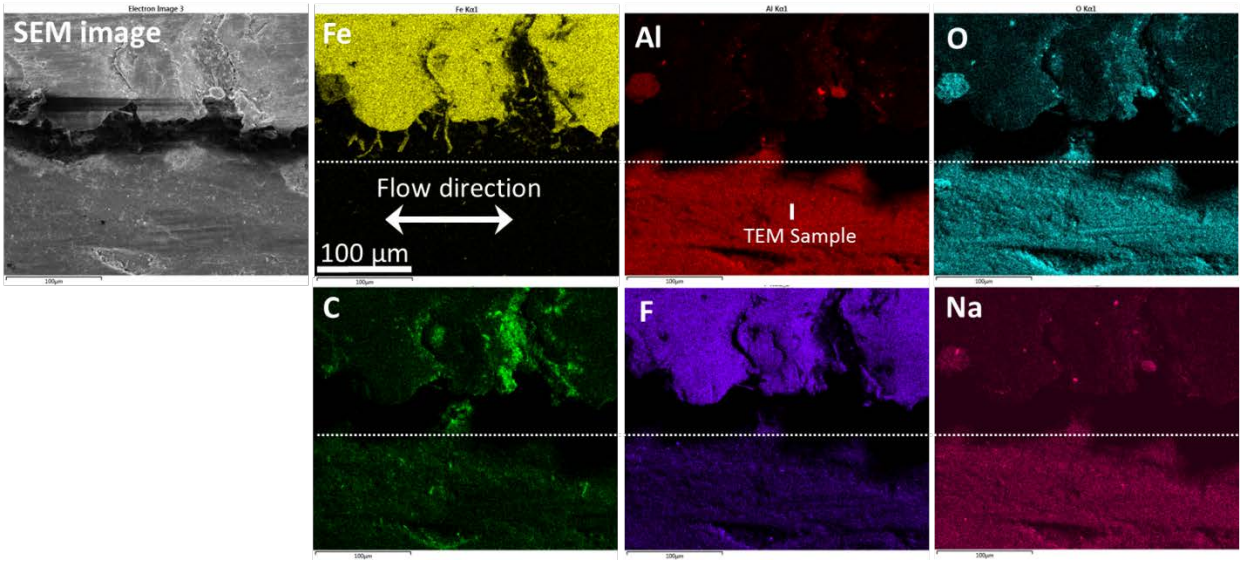

Figure 2: SEM image and EDS element maps of the pipe-scale interface. Also marked is the location of the TEM sample. The high concentration of F in the top part of the image that contain pure steel, is an artefact due to overlap between the F K- and the Fe L-peaks in the EDS spectra.

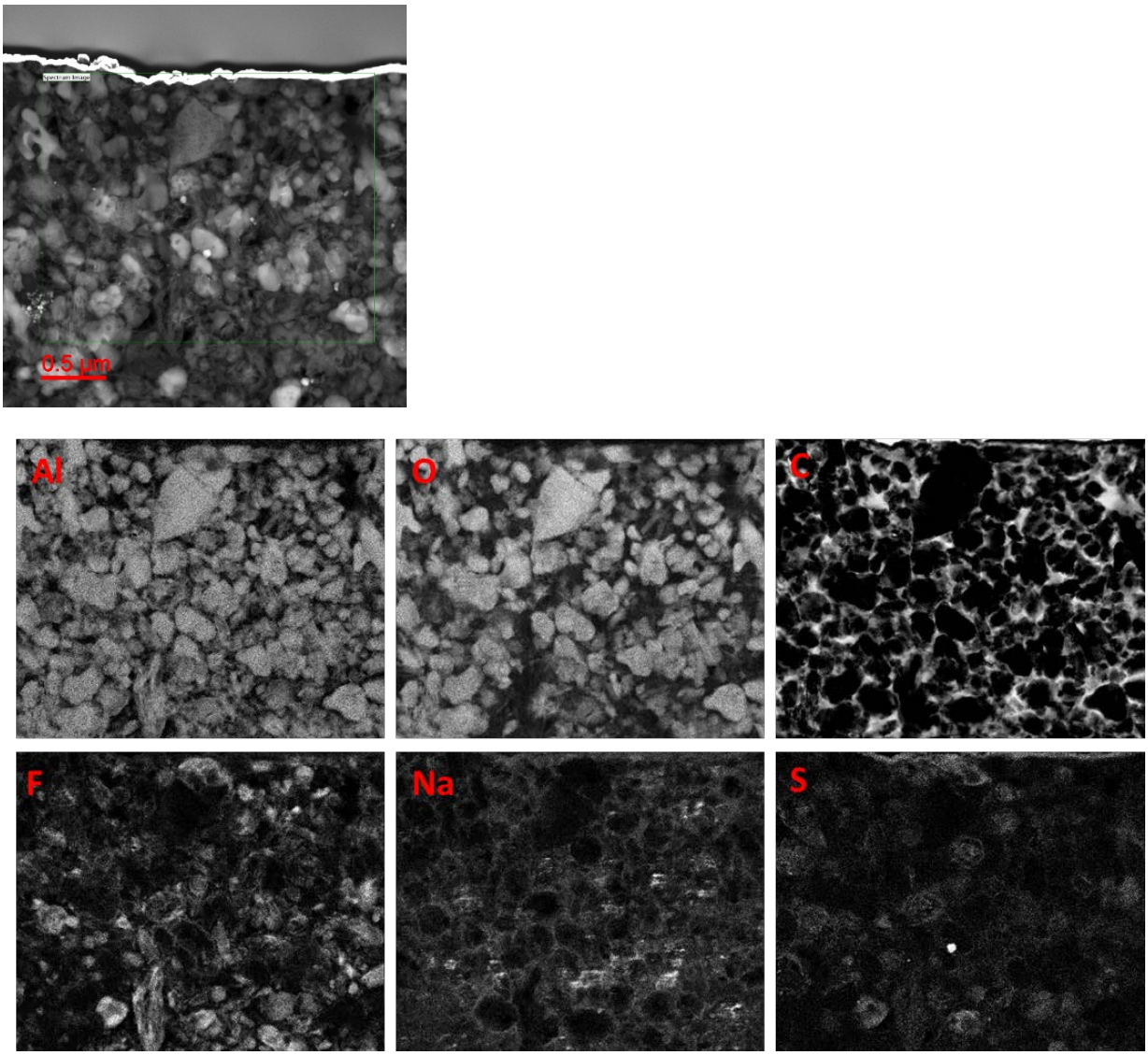

Figure 3: High angle annular dark field scanning transmission electron microscopy (HAADF STEM) image of the scale, with element mapping for the most interesting elements.

In Figure 3, a high angle annular dark field scanning transmission electron microscopy (HAADF STEM) image of the scale is shown. As TEM is a transmission technique, a 2D-image of the x-y plane will be seen, while differences along the z-direction (the direction of the electron beam) is lost due to averaging along this direction. This gives the effect that particles might seem closer together than they are since they might be offset in the z-dimension of the sample.

There is a lot of interesting information that can be found in this TEM image, and the associated EDS mappings. The grain size in this section was around 0.2-1 µm. The element distribution indicates that carbon and sodium is exclusively located at grain boundaries, while sulphur is present on the alumina grains. Likewise, aluminium and oxygen are mainly found in the alumina grains, smaller amounts could also be identified between the grains since the contrast is adjusted individually for each element. Fluorine is seen in high concentrations at some few of the larger alumina grains but most of the smaller alumina grains have little fluorine on them.

Using electron diffraction on the TEM made it possible to identify the crystalline structure of the grains in the sample. The main part of the alumina in the scale were identified as α-Al_2O_3, while some few γ-Al_2O_3 grains were found. γ- Al_2O_3 tended to be larger particles above 1 µm, although some smaller γ-Al_2O_3 were observed as well. The grains showing high contrast for fluorine were γ- Al_2O_3.

Between the Al_2O_3 grains, sodium, carbon and fluorine was identified by EDS. Since sodium carbide is not a likely phase to be found here, carbon could either be in the form of dust, or be present as Na_2CO_3 which could be

a reaction product formed from the Na_2O at the surface reacting with CO_2. Similar reactions with water could also give some NaOH. NaF would be the expected fluorine containing phase here, while $NaAlF_4$ or some other Na-Al-F phase could also be present depending on secondary reactions.

AFM measurements

Atomic force microscopy measurements give topology information in addition to information of the general physical properties of a surface, such as softness and adhesion. The analysis of the scale samples shows that there is a softer phase between the alumina grains, and that this soft phase has a significantly higher adhesion to the AFM probe than the alumina grains.

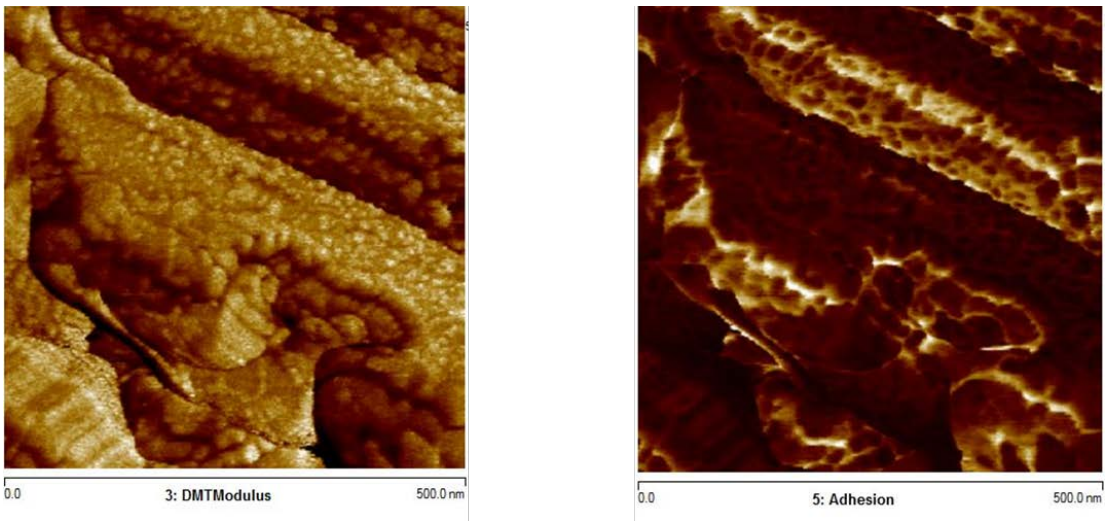

Figure 4: AFM showing surface hardness on the left, brighter is harder, and surface adhesion on the right, brigther is more adhersion.

Discussion

The main constituent of the scale is smaller (1um>) α-Al_2O_3 particles, while a few larger γ-Al_2O_3 particles is scattered around. The scale is enriched in sulphur (and possibly fluorine) compared to the secondary Al_2O_3 average contents.

There is no evidence of direct alumina-alumina bonding and no signs that could support the theory of geopolymer/hydraulic cement formation were found in this analysis. The individual alumina particles seem to be separated from each other, and no indication of neck formation was visible in any of the SEM or TEM pictures. In addition, the AFM measurements confirms that the fine fraction that fills the space between the alumina grains have a significant adhesion, and hence likely acts as a glue or binder between the alumina grains.

Despite the general enrichment of sulphur, a binder phase of sulphur or gypsum is unlikely in this case, as sulphur is not identified at the interface between the grains in the EDS mappings. Sulphur seems to be located on the actual alumina grains, and there is no obvious way sulphur could contribute to the scale formation based on the TEM images obtained.

The fluoride content is the factor that changes the most as the alumina passes through the dry scrubber, and it is shown that fluorides are present between the grains in the scale. Hence the fluorides are an obvious binder candidate. Through mechanisms similar to the solid state NaF-AlF_3 reactions proposed in [2], fluorides could possibly react further to form a solid binding phase around the fine alumina particles. This formation mechanism is supported by the results from the multivariate data analysis, where a correlation between increases in fluoride emissions and scaling rate was found.

NaOH or Na_2CO_3 are other candidates to form a binder phase, both could be formed in the dry scrubber as a reaction between Na_2O and H_2O or CO_2. Na_2CO_3 is unlikely to alone form any strong bonding phase, but NaOH has a low enough melting point that it could melt from the collision energy of the alumina in high turbulence zones and then solidify to act as a glue between the particles.

The gas temperature in and out of the GTCs, the outdoors temperature and the gas temperature from the cells were found to be correlated with scale growth, supporting the assumption that such temperatures are influencing the scale growth and indicating that temperature dependent chemical reactions could be a part of the scale formation mechanism.

It is unknown whether the high α phase content is a result of the fact that the alumina fines are often enriched in alpha [4], or if α-Al_2O_3 preferentially is trapped in the scale during formations. The presence of α-Al_2O_3 could be explained either by gamma reacting to α-Al_2O_3 or by the fact that α-Al_2O_3 is overrepresented in the particle distribution that is trapped in the scale. Findings in the multivariate data analysis indicated that the fines content in secondary alumina could be connected to scale growth.

The corrosion on the interface between the scale and the pipe was unexpected. It could be caused by a secondary reaction between moisture contained in the scale and the steel pipe. There are several corrosive elements such as HF present in the alumina that, when exposed to the steel for a prolonged time, could lead to corrosion.

Conclusions

Multivariate analysis of process and weather data obtained during a scale monitoring campaign indicated that the amount of emissions from the cells, cell temperature and/or gas temperature are important factors influencing scale formation. The fines contents in the alumina could also be an important factor. However, further studies are needed to validate these findings.

The examined scale samples were found to consist of mainly α-Al_2O_3 particles of sizes between 0.2 μm to 1 μm. Sodium, fluorine and carbon were mostly found between the grains, while oxygen and aluminium were found both between the grains and in the α-Al_2O_3. Sulphur was only found on the α-Al_2O_3 grains. Fluorine was observed at some of the grains, and these grains were later identified as γ-Al_2O_3.

A solid amount of work has been put into monitoring the HGS growth and studying its chemical composition. A significantly better understanding of the scale has been achieved, and although it has not been possible to conclude on any formation mechanism, sulphur, geopolymers and recrystallisation of alumina as has been ruled out as potential mechanisms.

Acknowledgment

Hydro Aluminium AS, Omya Hustadmarmor AS and GE Power Norway AS are thankfully acknowledged for financial support of this research project together with the Research Council of Norway (project no. 247789).

References

[1] Dando, NR, Lindsay, SJ (2008) Hard grey scale. In: Bearne, G, Dupuis, M, Tarcy, G (Eds) Essential Readings in Light Metals, Aluminium reduction technology. The Minerals, Metals & Materials Society, John Wiley & Sons, New Jersey, p 602-607

[2] Scholz, G, Korup, O (2006) High-energy ball milling – A possible synthesis route for cryolite and chaolite. Solid State Sci 8:678-684

[3] Wijayaratne, H, Hyland, M, Mcintosh, G, Perander, L, Metson, J (2018) Balancing sodium impurities in alumina for improved properties. Metall Mater Trans B, 1-12

[4] Perander, LM, Zujovic, ZD, Kemp, TF, Smith, ME, Metson, JB (2009) The nature and impacts of fines in smelter-grade alumina. JOM 61(11):33-39

[5] Gaertner, H (2013) Characteristics of particulate emissions from aluminium electrolysis cells. Ph.D Thesis, Norwegian University of Science and Technology

[6] Davidovits, J (2014) Geopolymer Chemistry & Applications, 4th ed. Saint-Quentin, Geopolymer Institute

[7] Mitchell, MB, Sheinker, VN, White, MG (1996) Adsorption and reaction of sulfur dioxide on alumina and sodium impregnated alumina. J. Phys. Chem. 100(18):7550-7557

[8] Zhang, X, Zhuang, G, Chen, J, Wang, Y, Wang, X, An, Z, Zhang, P (2006) Hetrogenous Reactions of Sulfur Dioxide on Typical Mineral Particles. J. Phys. Chem. B 110(25):12588-12596

[9] Fleer, M, Lorentsen OA, Harvey, W, Palsson, H, Saevarsdottir, G (2010) Heat recovery from the exhaust gas of aluminium reduction cells. In: Johnson, J (Ed) Light metals 2010. The Minerals, Metals & Materials Society, John Wiley & Sons, Warrendale, pp 243-248

[10] Østbø, NP (2002) Evolution of alpha phase alumina in agglomerates upon addition to cryolitic melts. Ph.D Thesis, Norwegian University of Science and Technology

[11] Haugland, IB, Halstensen, M (2017) Online acoustic chemometrics monitoring of scale deposition thickness in pneumatic conveying systems: A feasibility study. Paper presented at the 5th International Symposium of Reliable Flow of Particulate Solids (RELPOWFLO), Skien, Norway, 13-15 June 2017

[12] Haugland, IB, Halstensen, M (2018) A technique for obtaining reference measurements to calibrate deposition models for pipelines. Chem. Eng. Technol. doi: 10.1002/ceat.201700567

[13] Haugland, IB, Chladek, J, Halstensen, M (2018) Monitoring of scale formation in a pneumatic conveying system operating in a metal production plant. Submitted to Powder Technology

[14] Kvalheim, OM (1987) Latent-structure decompositions (projections) of multivariate data. Chemom. Intell. Lab. Syst. 2(4): 283-290

[15] Esbensen, KH (2001) Multivariate data analysis - in practice : an introduction to multivariate data analysis and experimental design, 2nd ed. Oslo: Camo

[16] Martens, H, Næss, T (1989) Multivariate calibration. Wiley, Chichester

[17] Andersen, CM, Bro, R (2010) Variable selection in regression – a tutorial. J. Chemom. 24(11-12): 728-737

[18] Sirius version 10.0, Pattern Recognition Systems AS, Bergen, Norway

[19] Yao, Y, Bao, J, Skyllas-Kazacos, M, Welch, BJ, Akhmetov, S (2018) Fault Detection and Diagnosis In Hall–Héroult Cells Based on Individual Anode Current Measurements Using Dynamic Kernel PCA. Metall Mater Trans B, 1-12

[20] Henry, JL, A Study of Factors Affecting Fluoride Emission from 10,000 Ampere Experimental Aluminum Reduction Cells. In: Bearne, G, Dupuis, M, Tarcy, G (Eds) Essential readings in light metals, Aluminium reduction technology. The Minerals, Metals & Materials Society, John Wiley & Sons, Inc. New Jersey, p 855-864

[21] Kalyavina, S, Ratvik, AP, Aarhaug, TA (2013) Impurities in Raw Gas and Secondary Alumina. In: Sadler, B (Ed) Light metals 2013. The Minerals, Metals & Materials Society, John Wiley & Sons, Inc. New Jersey, p 195-200